Check for updates

Imbibition on a porous layer: dynamical and mechanical characterization

Marguerite Léang, [ab] Ludovic Pauchard, [a] Lay-Theng Lee[b] and
Frédérique Giorgiutti-Dauphiné [*a]

Solvent penetration in porous layers was analyzed using dynamical and mechanical characterization. Spreading dynamics of a solvent drop in a porous substrate provided parameters of the porous medium such as permeability and porosity. These measurements are relevant for many porous systems, for example paintings or porous varnishes and resins... We present direct visualizations of the drop as well as of the wet zone during the imbibition process and we evidence three distinct regimes. Experiments performed with various porous systems and different solvents highlight a universal behavior. The mechanical properties during the imbibition process are deduced through indentation testing measurements. We show that solvent penetration is responsible for the appearance of a viscous component in the system. A characteristic time depending on the solvent and on the porous medium is then deduced. The system recovers its initial mechanical properties and no swelling nor cracking is observed contrary to the case of paintings. This result tends to prove that visco-plastic properties are required to observe swelling or cracking.

1 Introduction

The phenomenon of imbibition in porous media is widely encountered in industrial situations or in the domain of cultural heritage particularly when restauration operations are carried out to remove and to replace the varnish layer of a painting. Indeed, the most common treatment used by curators to remove varnish consists in using organic solvents[1] applied to solubilize the old varnish and to remove it. Generally, when a solvent penetrates in a porous layer, it can cause swelling or inversely a decrease of volume after solvent evaporation, and consequently, it can induce additional stresses on the matter which lead to the formation of cracks. In addition, the solvent can modify the interactions between the components of the porous medium and consequently implies modifications of the mechanical properties of the porous layer.

To prevent these undesirable effects, one needs to study the dynamics of solvent penetration in a porous substrate and the potential modifications induced on the matter such as: dissolution, variations of the mechanical properties, modifications of interactions between various components of porous medium or changes in the stress field due to swelling for example.

The aim of the presented work is to explain the physical mechanisms that come into play in imbibition processes and to identify physical macroscopic parameters, as relevant parameters, to describe the imbibition process for various porous systems which could be paintings, varnish or resins.

To this end, we propose to study the imbibition process of three different solvents in porous model systems formed after controlled drying of colloidal dispersions. The use of model systems has been motivated by the intent to deal with a well known and controlled system.[2] The problem of solvent imbibition process on a porous medium has been studied by various authors; the widely used geometry is the case of a liquid droplet deposited on a porous substrate. Different situations have been addressed: the case of a porous medium partly or entirely filled with liquid,[3,4] the case of a drop whose size is small or comparable to the size of the porous layer.[5] The wetting properties, the viscosity of the liquid or its volatility are the main parameters considered. Each parameter will play a role on respectively the spreading of the drop, the viscous flow in the drop or/and the diffusion in the porous and the evaporation. Davis *et al.*[6] and then Alleborn *et al.*[7] used lubrication theory combined with Darcy's law to model spreading and sorption of a two-dimensional drop on a dry or saturated porous substrate. They obtained numeric profiles of the drop and of the wet zone, during the imbibition process. Some authors have included dynamic contact angle and contact angle hysteresis in their model or some employed Brinkman's equation to solve the flow in the porous medium.[8,9] Nevertheless, there are very

[a] *Laboratoire F. A. S. T., Univ. Paris-Sud, CNRS, Université Paris-Saclay, F-91405, Orsay, France. E-mail: fred@fast.u-psud.fr*

[b] *Laboratoire Léon Brillouin, UMR12 CEA-CNRS, Bât. 563 CEA Saclay, 91191 Gif sur Yvette Cedex, France*

few experimental visualizations, to our knowledge, of both the drop and the wet zone in the porous medium during the imbibition process.[10,11] In the present work, we propose an experimental study of the imbibition process based on direct visualization of simultaneously spreading and sorption of a drop on a porous substrate. The experimental profiles validate the numerical results obtained by solving both the lubrication and Darcy's equations in the work of Alleborn and Raszillier (2004). We performed experiments with three different solvents and two porous media and founded a universal behavior for the imbibition dynamics. In addition, we can estimate permeability of the porous substrate in two directions: parallel and perpendicular to the flow. We then present then indentation measurements conducted on the porous substrate before and after imbibition process to measure the impact of solvent penetration on the mechanical properties of the porous layer. Finally, we estimate dissolution of the porous media due to imbibition process.

2 Imbibition dynamics

2.1 Material and methods

The porous media of interest in this work are obtained during the drying of aqueous dispersions of silica colloidal particles: Ludox SM-30 and HS-40 commercially available from Sigma-Aldrich. The radius of silica particle is noted a and the initial particle volume fraction is $\phi_{p,0}$ (see Table 1). The pH value is in the range of 9–10 to ensure that a high negative charge density is born by the particles; the DLVO theory is expected to apply and the dispersions are used without previous treatment. A liquid layer is formed by depositing a controlled volume of dispersion in a non-porous substrate (glass Petri dish), then the layer is left to dry from the free surface. The relative humidity is kept constant, RH = 54 $\pm$ 2%, at room temperature. Solvent evaporation concentrates the dispersion until the formation of a porous layer of approximately constant thickness in the centre of the container. The volume of dispersion initially deposited is chosen to obtain a solid layer thickness of around 1 mm.

As drying proceeds, shrinkage is frustrated by adhesion with the substrate. It causes large tensile stresses which lead to the formation of cracks which divide the layer into polygonal adjacent fragments. These fragments have been characterized through neutron imaging techniques to deduce the porosity $1 - \phi_p$ of their structure, where ϕ_p is the particle volume fraction.

The permeability $\mathcal{K}$ is deduced from the Kozeny–Carman law based on the size of the nanoparticles.[12,13] The main properties of the porous structure are reported in Table 1. One should note that we have considered fragments with no cracks as the presence of cracks will enhance and modify solvent penetration.

Three kinds of solvents are imbibed into the porous layers: water, ethyl acetate and glycerol. The choice of water and ethyl acetate has been motivated given their ordinary use by curators. Glycerol is not used in restoration but is a limiting case for the model due to its high viscosity and non-volatility. We have reported the main properties of the different solvents at $T = 20$ °C in Table 2.

The experimental setup used to follow the dynamics of imbibition is presented in Fig. 1. A fragment of uniform thickness is selected. The thickness of a fragment is measured by successively focusing on the top (air–layer interface) and on the bottom (layer–substrate interface) of the deposited film in transmitted light. The accuracy of this method is to within 3 μm. Horizontality is adjusted by 3 screws on the sample holder. The experimental set-up allows us to image a fragment and provides both side and top view using two cameras (Marlin F131B, Allied Vision Technologies). Acquisition frequency is 1.875 frame per second (fps) for glycerol imbibition dynamics, whereas for water and ethyl acetate, we used a fast-speed

Table 2 Main characteristics of the solvents used for imbibition processes at $T = 20$ °C. M_W is the molecular weight; ρ, the density; γ, the surface tension and η, the dynamic viscosity[14,15]

Solvent	M_W (g mol^{-1})	ρ	γ (mN m^{-1})	η (mPa s)
Water	18	1	72.8	1
Ethyl acetate	88.1	0.9	23.9	0.46
Glycerol	92	1.26	63	1499
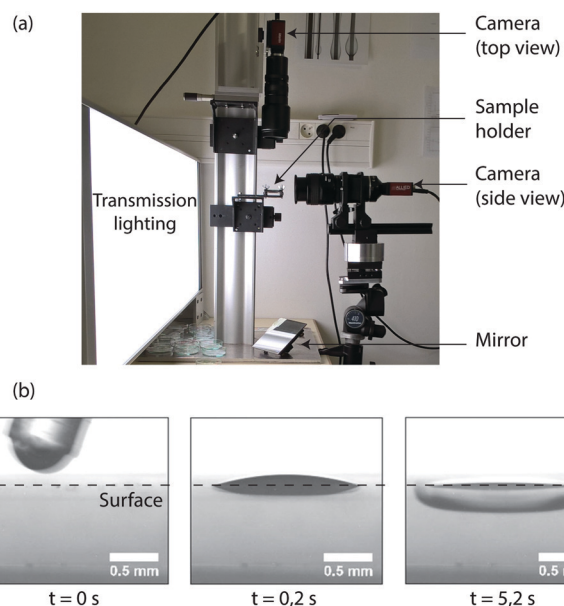
Fig. 1 (a) Experimental set-up composed of a sample holder, two cameras which acquire transmitted images. (b) Successive images during the imbibition of a glycerol drop on a porous system formed by drying Ludox HS-40.

Table 1 Main properties of silica dispersions (particle diameter $2a$) and porous media. $\phi_{p,0}$ is the initial particle volume fraction of the dispersions. The volume fraction of the voids in the porous media is denoted $1 - \phi_p$ with ϕ_p, the particle volume fraction. The values have been determined by neutron imaging; $\mathcal{K}$ is the permeability calculated from Kozeny–Carman law.[12,13] Measurements uncertainties are averaged over three different samples

	Colloidal dispersion			Porous medium	
System	$2a$ (nm)	$\phi_{p,0}$	pH	$1 - \phi_p$	$\mathcal{K}$ (m^2)
SM-30	10	0.15 ± 0.04	9.9	0.33 ± 0.02	2×10^{-20}
HS-40	16	0.22 ± 0.01	9.8	0.31 ± 0.03	3.7×10^{-20}

Table 3 Comparison of Darcy's time, t_{Darcy} as a function of solvents and of porous media HS-40 and SM-30. V_E is the evaporation rate. The drying timescales t_D is defined as: $t_D = L_{\text{imb}}/V_E$ where $L_{\text{imb}} = 100$ µm is a typical length for drop penetration in the porous media

| Porous	HS-40	SM-30		
Solvent	t_{Darcy} (s)	t_{Darcy} (s)	V_E (m s^{-1})	t_D (s)
Water	10	11	5×10^{-8}	2000
Ethyl acetate	13	15	1×10^{-7}	1000
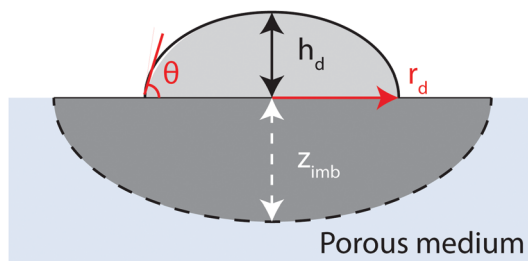
Fig. 2 Scheme of the drop on the porous substrate: definition of the experimentally measured lengths: r_d is the drop radius, h_d is its height at the drop centre, θ is the drop contact angle with the porous medium. Inside the porous medium, z_{imb} is the vertical penetration depth at the centre of the drop.

camera Eo Sens 6546 CF 25-290 (Mikrotron GmbH) with a 200 fps frequency. A drop of a given volume is then deposited with a micropipette (Fisherbrand). The drop characteristic size is smaller than the capillary length ensuring an initial spherical cap shape for the sessile drops. The imbibition process takes place during a low duration in comparison with the evaporation timescale t_D, less than <1/100 (see Table 3). Thus, the whole drop that is deposited is assumed to penetrate into the porous layer. The drop and the wet area in the porous medium are illuminated by transmitted light, simultaneously. The two main advantages of the setup are the following. Firstly, the wet region can be followed with time by imaging successive profiles (see images in Fig. 1). Secondly, the axisymmetry of the deposited sessile drop and the wet region are easily followed using the top-view camera. Hence, the quantification of the profiles of both the sessile drop and the imbibed region reveals the conservation of the volume of liquid all along the imbibition process. This important point allows us to determine the volume of the imbibed region at each time.

The main parameters involved during the drop imbibition are reported in Fig. 2: the drop radius r_d (the maximum radius is $r_{\text{dmax}} = r_d(t_0)$, reached at time t_0), the drop contact angle θ (the initial contact angle is noted θ_0), the vertical penetration depth z_{imb} at the center of the drop. h_d is the drop height at its center, and the initial drop height is $h_{d,0}$.

2.2 Dynamics of drop imbibition

The same scenario is observed for the three used solvents and both porous media: the imbibition process can be decomposed in three distinct stages. In the first stage, the drop spreads on the porous fragment; the drop radius increases whereas the
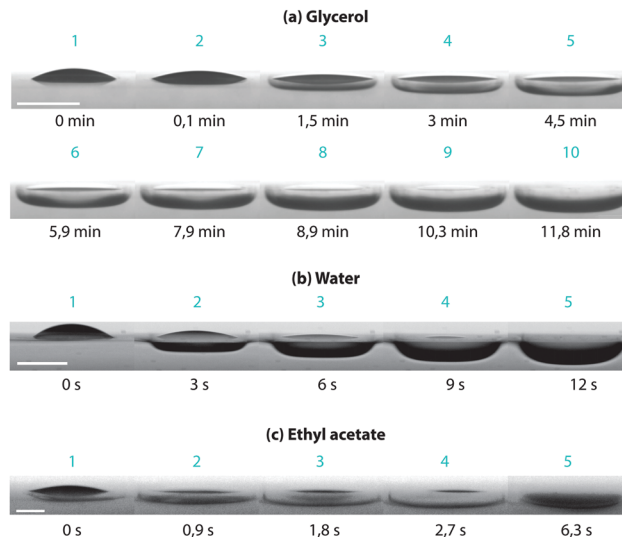

Fig. 3 Evolution of a drop of three solvent spreading and then imbibing porous fragment of Ludox HS-40 (particle radius $a = 8$ nm). (a) The initial volume of glycerol drop: 0.1 µL. (b) The initial volume of water drop: 0.2 µL. (c) The initial volume of ethyl acetate: 0.08 µL. Scale bar: 1 mm.

contact angle decreases (images 1–3 in Fig. 3(a) for glycerol). In a second step, the surface area of the drop contact base is constant: the contact line is pinned by surface defects and the contact angle still decreases (see images from 3 to 4 in Fig. 3(a)). Simultaneously, the solvent starts penetrating in the porous. Both radii, respectively of the drop and of the wet area are the same. In the last stage, the drop is no more pinned and its radius decreases as well as its contact angle. The radius of the wet area remains constant and equal to the maximum value of the drop radius whereas the vertical penetration increases (see Fig. 3(a), images from 4 to 10). At the end of the process, there is no more solvent outside the porous and the wet area is axisymmetric.

The time variations of the dimensionless drop radius, r_d/r_{dmax}, and dimensionless contact angle, θ/θ_0, are plotted in Fig. 4 for different initial drop volumes. Note that time t_0 corresponds to the end of the spreading stage of the drop and is chosen as a time reference.

We observe a brutal change of the slope for the drop radius correlated with the contact angle. These curves attest of a good reproducibility of the process. The data for experiments on two porous and with three solvents have been scaled with the Darcy's time, t_{Darcy}, defined as the time for the drop to penetrate in the porous medium, hence:[16] $t_{\text{Darcy}} = \eta h_d^2(t_0)(1 - \phi_p)/\mathscr{K}P_{\text{cap}}$ with η the viscosity of the solvent; $h_d(t_0)$, the height of the drop when the drop radius is maximum (at the end of the spreading stage t_0); $(1 - \phi_p)$ is the porosity of the medium; $\mathscr{K}$ is the permeability determined by neutron imaging (see values in Table 1) and P_{cap} is the capillary pressure which is the pressure of liquid in the pores of the system. Here, we take $P_{\text{cap}} \sim \dfrac{\gamma}{a}$ where γ is the solvent superficial tension and a, the particle radius.[17] For water with HS-40 and SM-30 porous media, we found 9.3×10^6 Pa $\leq P_{\text{cap}} \leq 1.5 \times 10^7$ Pa whereas for ethyl
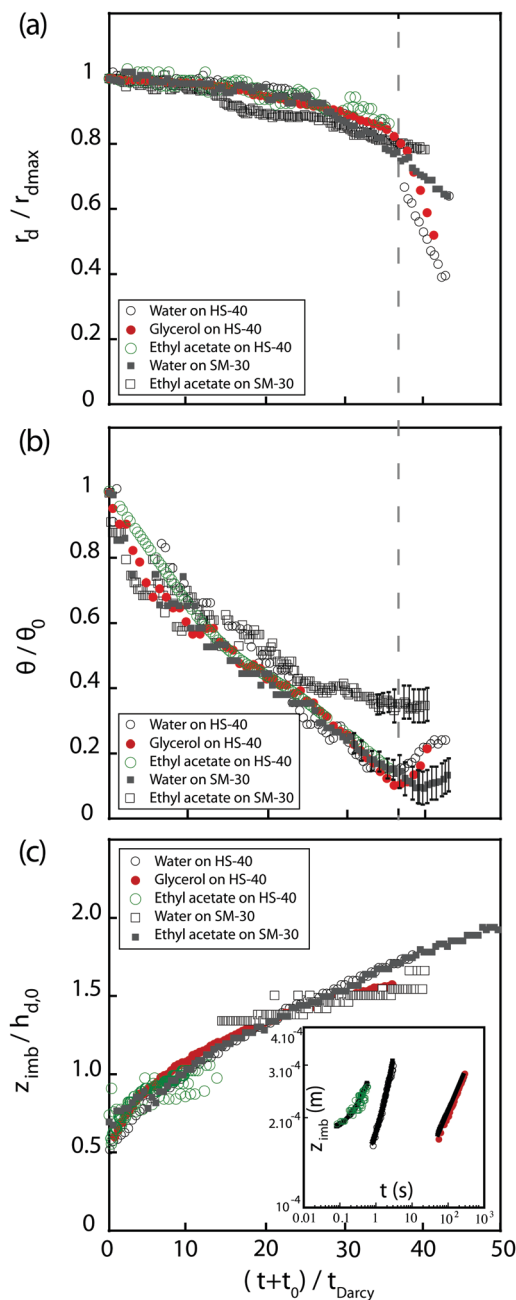
Fig. 4 (a) Time evolution of the dimensionless drop radius, $r_d/r_{d,max}$, contact angle, θ/θ_0, and vertical penetration, $z_{imb}/h_{d,0}$, with the dimensionless time $(t + t_0)/t_{Darcy}$, where t_0 corresponds to the end of the drop spreading stage. Colours: different solvents penetrating in different porous media. Vertical dotted line: drop radius change is correlated to drop contact angle change. Inset: z_{imb} as a function of time, log–log scale. The initial contact angle, θ_0, of water, glycerol and ethyl acetate on the porous surfaces are $31 \pm 2°$, $20 \pm 2°$ and $18 \pm 2°$, respectively.

acetate with HS-40 and SM-30 porous media, 3×10^6 Pa $\leq P_{cap} \leq 5 \times 10^6$ Pa. Table 3 shows values of t_{Darcy} for water and for ethyl acetate on HS-40 and SM-30 porous.

Note that for a kind of porous, Darcy's time of ethyl acetate is bigger than those of water. A possible explanation can be capillary condensation in the pores.[18] In fact, ethyl acetate evaporates faster than water and condensation of ethyl acetate vapour can take place in the void spaces. This can modify the wettability of the silica particle surface. Thus, ethyl acetate penetrates faster and easier in the porous media than water, leading to a bigger imbibition speed inside the porous media. The drying timescale t_D is defined as the drop mean height divided by the solvent evaporation rate V_E, for constant relative humidity. This evaporation rate has been measured by the mass loss with time of a volume of 5 mL, in a Petri dish, at ambient temperature and with a relative humidity of 50%.[19] A typical length for drop penetration is $L_{imb} = 100$ μm. Table 3 shows the evaporation rate for water and ethyl acetate and the corresponding drying timescales.

All the curves collapse into a universal imbibition curve when plotted with the scaling time t/t_{Darcy}. A deviation is observed for dimensionless times about 10; at that time, the drop is very small and the resolution of the corresponding images do not provide enough precisions on the drop profiles. We have plotted as well, the height of the wet area z_{imb}, scaled with the height of the initial drop $h_{d,0}$. Again a universal behavior is evidenced.

The porosity values of the different porous media were deduced from neutron imaging techniques. We used a cold neutron imaging spectrometer. It allows performing radiography and tomography with fields of view ranging from 20 to 100 mm using a CMOS ANDOR NEO camera. Radiography can be performed with a field of view of 200×400 mm^2 by using a FUJI image plate. The incident neutron beam has a diameter of 20 mm, with a wavelength between 2 and 30 Angstrom. The spatial resolution is between 100 and 130 micrometers. The neutron beam passes over the sample (a fragment of the porous medium, obtained by drying, with a uniform thickness over the whole fragment) and we measured the transmitted light on an image formed thanks to a scintillator and a camera. By dividing the transmitted light of a sample filled with water with the transmitted light of a dry sample, we obtained the thickness of the sample traversed by the neutron beam and we deduce, knowing the total thickness of the sample, its porosity.

Another key parameter of the porous medium is the permeability which can be deduced from two different ways: using the Kozeny–Carman law or by direct measurements. This last method is based on the dynamics of the imbibition front depicted by the spatiotemporal diagrams presented on Fig. 5. We have recorded with time the vertical and the horizontal dashed lines to produce spatiotemporal diagrams of respectively the vertical and the radial imbibition front in the porous medium. We deduce the temporal evolution of the wet area z_{imb} and its radial spreading r_{imb}. At the beginning of the imbibition process, evolutions of the fronts are linear and then become proportional to $\sqrt{t}$ to finally saturate. This behavior is similar to the dynamic of the capillary rise[20] as the liquid penetration in the porous medium is due to a pressure gradient in the pores of the system, that is the capillary pressure. There are then three stages in the capillary rise dynamics which depend on the dominant physical mechanisms. The first stage is a regime dominated by the inertial forces, then the second regime is called the
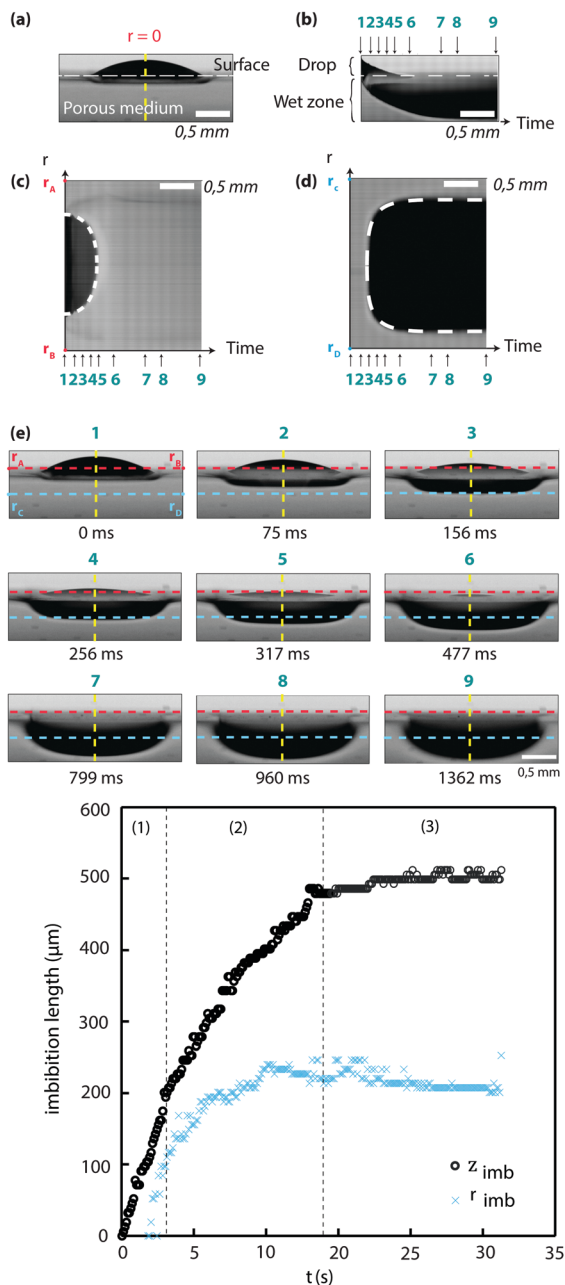
Fig. 5 Time evolution of vertical and the radial fronts. (a) Side view of a drop deposited on the surface of a porous medium. (b) Spatio-temporal diagram along the yellow dashed line, $r = 0$, in (a). (c) and (d) Spatio-temporal diagrams obtained along the red and the blue horizontal lines represented in (e), *i.e.* in the drop, and in the wet zone. (e) Images of the drop imbibition at different times. The numbers in (b)–(d) correspond to the images in (e). Scale bar: 0.5 mm. (f) Position for the imbibition front with time in vertical and radial directions; the Washburn regime corresponds to the zone (2).

Washburn's regime where inertial forces become negligible compared to the viscous ones. The evolution of the imbibition front in the case of a porous medium is then given by:[21,22]

$$z_{\mathrm{imb}} = \sqrt{\frac{\gamma \, \cos(\theta_{\mathrm{p}}) r_{\mathrm{eff}}}{2\eta T^2}} \sqrt{t} \qquad (1)$$

Table 4 Comparison or mean pore radius determined by Washburn's law for vertical and radial imbibition dynamics of a drop inside 2 porous media and mean pore radius determined by neutron imaging

Neutron imaging

Porous media	a (nm)	Porosity $1 - \phi_{\mathrm{p}}$	κ_{KC} (m^2)	κ_{Bear} (m^2)
Ludox SM-30	4.8	0.33	2.0×10^{-20}	2.0×10^{-20}
Ludox HS-40	7.9	0.31	3.7×10^{-20}	4.6×10^{-20}

Sessile drop imbibition

Porous media	Vertical dynamics		Radial dynamics	
	$r_{\mathrm{eff}}^{\mathrm{vert}}$ (nm)	$\kappa_{\mathrm{Bear}}^{\mathrm{vert}}$ (m^2)	$r_{\mathrm{eff}}^{\mathrm{radial}}$ (nm)	$\kappa_{\mathrm{Bear}}^{\mathrm{radial}}$ (m^2)
Ludox SM-30	1.66	2.7×10^{-20}	3.0	8.0×10^{-20}
Ludox HS-40	1.80	2.9×10^{-20}	4.0	1.5×10^{-19}

a: particle radius composing the porous media, κ_{KC}: Kozeny–Carman permeability, κ_{Bear}: Bear's law permeability. $r_{\mathrm{eff}}^{\mathrm{vert}}$, $\kappa_{\mathrm{Bear}}^{\mathrm{vert}}$: vertical imbibition, mean pore radius and Bear's permeability respectively; $r_{\mathrm{eff}}^{\mathrm{radial}}$, $\kappa_{\mathrm{Bear}}^{\mathrm{radial}}$: radial imbibition, mean pore radius and Bear's permeability respectively.

with γ, the solvent surface tension; θ_{p}, the contact angle between solvent and particle surface (θ_{p} is taken to be zero due to silica particle hydrophilicity); r_{eff}, the effective radius of the porous and T, the tortuosity. The tortuosity is deduced from the porosity values through the relation:[23–25] $T = 1/\sqrt{1 - \phi_{\mathrm{p}}}$ and the permeability expresses as: $\mathcal{K} = (1 - \phi_{\mathrm{p}})/24Tr_{\mathrm{eff}}^2$, which is given by Bear.[26] By fitting the curves (6f) representing the evolution of the imbibition front with time, with the Washburn's law, one can deduce the value of r_{eff}. The results have been compared to values obtained with neutron imaging techniques (Table 4) and are equivalents (the experiment, in that case, consists of recording the imbibition front in a vertical fragment whose one end is in contact with a water bath).[27] It turns out that the effective radius is always lower than the particle size, a, typically of factor 3 for the different colloidal systems we used. In the case of the sessile drop experiment, the fit of the curves in 6f with the Washburn's law, provides expressions for the two permeabilities in the two directions vertical and radial ones, respectively, $\mathcal{K}_{\mathrm{vertical}}$ and $\mathcal{K}_{\mathrm{radial}}$. The results are reported in Table 4. The permeability in the radial direction $\mathcal{K}_{\mathrm{radial}}$ is always higher than the one in the vertical direction $\mathcal{K}_{\mathrm{vertical}}$. This observation can be related to results of previous work with the same systems in SANS experiments.[28] It has been shown that particles are closer in the direction of the drying flux, consequently, permeability of the final porous medium should be lower in this direction. These results are confirmed with our experimental values: $\mathcal{K}_{\mathrm{vertical}} \leq \mathcal{K}_{\mathrm{radial}}$. This suggests a non completely homogeneous porous medium, due to the vertical drying flux conducting to vertical compression of particles.

3 Evolution of the mechanical properties before and after drop imbibition

The mechanical properties of a porous medium strongly depend on its moisture content. This section is devoted to compare
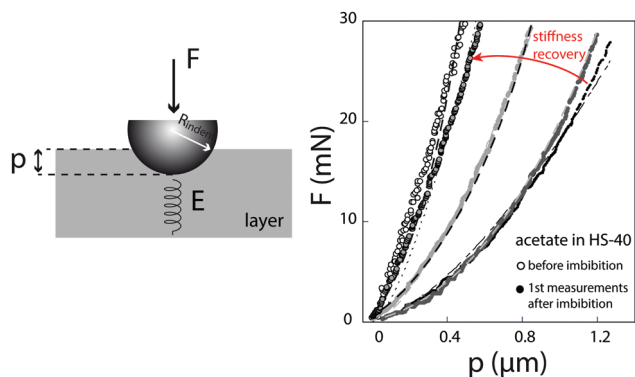
Fig. 6 Spherical indentation load-displacement (applied force F *vs.* penetration depth p) in HS-40 porous layers. The present test shows a series of measurements performed before imbibition (°). Then each series of dots correspond to an indentation load-displacement performed after ethyl acetate imbibition and during the stiffness recovery. The measurements (dots) are fitted by dashed lines according to eqn (2).
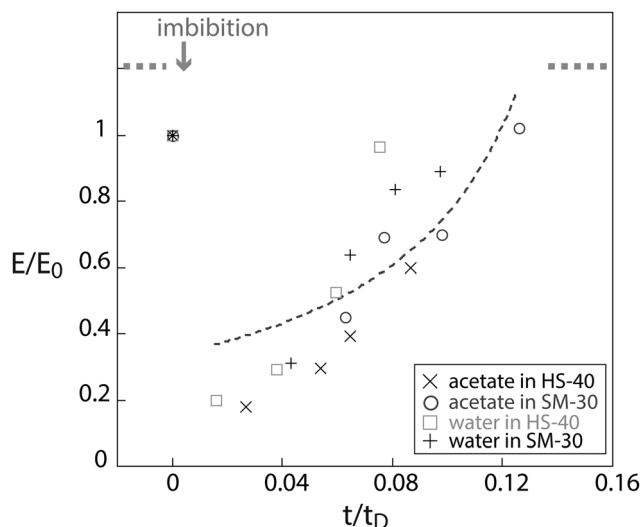

Fig. 7 Evolution of the dimensionless elastic modulus, E/E_0, as a function of the dimensionless time, t/t_D, for different porous media (HS-40 and SM-30) after imbibition by ethyl acetate or water. E_0 is the elastic modulus before drop imbibition ($E_0 = 1.1 \pm 0.6$ GPa); t_D is the drying timescale. The moment of the imbibition process is indicated by the arrow. The dashed line corresponds to the theoretical predictions according to eqn (3).

the elastic behavior of a porous medium before and after drop imbibition. In this way measurements using indentation testing (CSM Instrument Micro-Hardness Tester – Anton Paar) were investigated on HS-40 and SM-30 layers of 1 mm thick. A typical experiment consists in the measurement of an applied force, F, using a spherical indenter (Rockwell indenter of radius $R_{indent} = 200$ μm) as a function of the penetration depth, p, as shown in Fig. 6. The maximum penetration depth of the indenter is always smaller than the solvent penetration depth (≈ 500 μm), except at the end of solvent evaporation from the porous media.

Assuming the material purely elastic within the limits of small deformations, the elastic response is well fitted using the Hertz contact law over a range of indentation depth such as $p < 1.2$ μm (Fig. 6). Hence, according to the classical Hertzian model, the applied indentation force F is determined by:[29]

$$F = \frac{4\sqrt{R_{indent}}}{3} \frac{E}{1 - \nu^2} p^{\frac{3}{2}} \qquad (2)$$

with the Poisson ratio $\nu = 0.2$.[30] Typical elastic behavior of a porous medium before drop imbibition is shown in Fig. 6. It has to be noted, the water moisture content in the porous layer is not zero since the humidity rate of the surroundings is finite. Within the first minutes following the drop deposition, measurements using indentation testing do not allow us to estimate elastic response. Once the drop is totally penetrated inside the layer, measurements are possible in the wet region. The load-displacement measurements are then characteristic of a low elastic modulus. Further measurements show recovery with time of the elastic behavior of the porous layer (Fig. 6). Fig. 6 reports the case of ethyl acetate imbibition into HS-40 porous layers. Similar behaviors are obtained with SM-30 porous layers and with water imbibition, the timescales involved being different. The elastic moduli which are deduced from load-displacement curves and eqn (2), are shown in Fig. 7. Using the poroelastic theory it has been shown that the drying stress linearly increases with time.[31] However, this model stated a

constant elastic modulus with time. The recovery with time of the elastic behavior can be pointed out by the following simple arguments. Consider X being the current moisture content of the porous medium after drop imbibition. E_0 is the elastic modulus of the medium without solvent content addition, the linearity between stress, σ, applied to the porous medium and its strain, ε_0, writes: $\sigma = E_0\varepsilon_0$ in the conditions of applicability of the Hooke's law. We observe no swelling of the material when water penetrated into the porous media, however, there is an additional deformation $\varepsilon(X)$ due to imbibition that we assumed to be proportional to the quantity of solvent which has penetrated in the porous medium. The degree of solvent saturation affects thus the elastic response of the porous medium and this results in larger strain, $\varepsilon + \varepsilon(X)$, and specific elastic modulus, $E(X)$, such as: $\sigma = E(X)(\varepsilon_0 + \varepsilon(X))$. The solvent molecules and silica structures are assumed to be incompressible. Consequently, the strain resulting from the moisture content can be written: $\varepsilon(X) = \varepsilon_0 \mathscr{V} X$ where $\mathscr{V}$ is the volume per solvent molecule. The evaporation rate of the solvent is assumed to be constant during the main solvent removal period and is defined as: $V_E = -\dfrac{\mathscr{V}}{S_0}\dfrac{dX}{dt}$ where S_0 is the evaporation surface. Finally the experimental results can be fitted by the law:

$$E(X)/E_0 = 1/(1 + \alpha(1 - t/t_D)) \qquad (3)$$

where α is a coefficient of the influence of the moisture content on the elastic properties of the material.[32] This highlights the effect of solvent evaporation in the timing recovery of the elastic behavior of a porous medium previously imbibed. In order to observe swelling and cracking as a result of solvent imbibition and solvent evaporation, visco-plastic properties seem to be required.[32–34]

4 Conclusion

We investigated the imbibition dynamics of three different solvents on two porous media. These porous media were characterized previously by neutron imaging. We implemented a set-up which permitted us to (i) verify the axisymmetry of deposited drops from a top view; (ii) to follow the drop profiles and the liquid front profiles inside the porous media. We described the imbibition dynamics by quantifying the drop radius, the drop contact angle, and the vertical penetration depth at the centre of the drop. A relevant characteristic time for imbibition is determined to be Darcy's timescale: a universal behavior for different solvents and porous media is shown. These dynamics are completed with mechanical properties of porous media, before and after imbibition. Particularly, viscoelasticity was measured by creep measurements and show different characteristic times for water and ethyl acetate. Moreover, the fitting of micro-indentation loading curves with the Hertz's contact law permitted the determination of Young's modulus of the porous media before and after drop imbibition. A recovery of mechanical properties was evidenced as solvent evaporated. This result tends to prove that visco-plastic properties are required to observe swelling or cracking.

Conflicts of interest

There are no conflicts to declare.

Acknowledgements

References

1 N. Stolow, *Recent advances in conservation: contributions to the IIC Rome conference*, 1961, pp. 84–88.

2 F. Giorgiutti-Dauphiné and L. Pauchard, *J. Appl. Phys.*, 2016, **120**, 065107.

3 V. M. Starov, S. R. Kosvintsev, V. D. Sobolev, M. G. Verlarde and S. A. Zhdanov, *J. Colloid Interface Sci.*, 2002, **246**, 372.

4 V. Starov, S. Zhdanov, S. Kosvintsev, V. Sobolev and M. Velarde, *Adv. Colloid Interface Sci.*, 2003, **104**, 123–158.

5 V. M. Starov, S. A. Zhdanov and M. G. Velarde, *Langmuir*, 2002, **18**, 9744–9750.

6 S. H. Davis and L. M. Hocking, *Phys. Fluids*, 2000, **12**, 1646.

7 N. Alleborn and H. Raszillier, *Chem. Eng. Sci.*, 2004, **59**, 2071–2088.

8 M. Hilpert and A. Ben-David, *Int. J. Multiphase Flow*, 2009, **35**, 205–218.

9 *Wetting and spreading dynamics*, ed. C. Press, V. M. Starov, M. G. Velarde and C. J. Radke, 2007.

10 S. Ogawa and J. Nakamura, *J. Opt. Soc. Am. A*, 2015, **32**, 2397–2406.

11 J. Lee, A. Radu, P. Vontobel, D. Derome and J. Carmeliet, *J. Colloid Interface Sci.*, 2016, **471**, 59–70.

12 J. Kozeny, Über kapillare leitung des wassers im boden: aufstieg, versickerung und anwendung auf die bewässerung, Hölder-Pichler-Tempsky, 1927.

13 P. C. Carman, *Chem. Eng. Res. Des.*, 1997, **75**, S32–S48.

14 *CRC Handbook of Chemistry and Physics*, ed. E. R. Weast, CRC Press, 56th edn, 1975–1976.

15 M. L. Sheely, *Ind. Eng. Chem.*, 1932, **24**, 1060–1064.

16 Z. Liu, Y. Wang, F. J. Muzzio, G. Callegari and G. Drazer, *Langmuir*, 2017, **33**, 56–65.

17 W. P. Lee and A. F. Routh, *Langmuir*, 2004, **20**, 9885–9888.

18 L. Bacri and F. Brochard-Wyart, *Eur. Phys. J. E: Soft Matter Biol. Phys.*, 2000, **3**, 87–97.

19 F. Boulogne, F. Giorgiutti-Dauphiné and L. Pauchard, *Oil Gas Sci. Technol.*, 2014, **69**, 397–404.

20 J. Bico, PhD thesis, Université Paris VI, 2000.

21 F. A. L. Dullien, *Porous Media: Fluid Transport and Pore Structure*, Academic press, San Diego, CA, 1979.

22 R. Hassanein, H. O. Meyer, A. Carminati, M. Estermann, E. Lehmann and P. Vontobel, *J. Phys. D: Appl. Phys.*, 2006, **39**, 4284.

23 Y. Bernabé and A. Revil, *Geophys. Res. Lett.*, 1995, **22**, 1529–1532.

24 P. W. Glover, I. I. Zadjali and K. A. Frew, *Geophysics*, 2006, **71**, F49–F60.

25 P. W. Glover and E. Walker, *Geophysics*, 2009, **74**, E17–E29.

26 J. Bear, *Dynamics of fluids in porous media*, Dover Publication Inc., New York, 1988.

27 M. Léang, PhD thesis, Paris-Saclay University, 2017.

28 F. Boulogne, L. Pauchard, F. Giorgiutti-Dauphiné, R. Botet, R. Schweins, M. Sztucki, J. Li, B. Cabane and L. Goehring, *EPL*, 2014, **105**, 38005.

29 A. C. Fischer-Cripps, *Nanoindentation*, Springer New York, New York, NY, 2004, pp. 1–20.

30 E. Di Giuseppe, A. Davaille, E. Mittelstaedt and M. François, *Rheol. Acta*, 2012, **51**, 451–465.

31 F. Giorgiutti-Dauphiné and L. Pauchard, *Eur. Phys. J. E: Soft Matter Biol. Phys.*, 2014, **37**, 39.

32 S. Kowalski, *Chem. Eng. J.*, 2002, **86**, 145–151.

33 S. M. Wiederhorn, T. Fett, J.-P. Guin and M. Ciccotti, *Int. J. Appl. Glass Sci.*, 2013, **4**, 76–86.

34 M. Liu and C. Chen, *Int. J. Solids Struct.*, 2015, **63**, 32–38.